

See discussions, stats, and author profiles for this publication at: <https://www.researchgate.net/publication/351635701>

An Extreme Heat Event Induced by Typhoon Lekima (2019) and Its Contributing Factors

Article in *Journal of Geophysical Research: Atmospheres* · May 2021

DOI: 10.1029/2021JD034760

CITATIONS

10

READS

424

4 authors, including:



Dingchi Zhao

Tsinghua University

9 PUBLICATIONS 34 CITATIONS

[SEE PROFILE](#)



Yanluan Lin

Tsinghua University

175 PUBLICATIONS 4,860 CITATIONS

[SEE PROFILE](#)



Yuanlong Li

Nanjing University

24 PUBLICATIONS 277 CITATIONS

[SEE PROFILE](#)

JGR Atmospheres

RESEARCH ARTICLE

10.1029/2021JD034760

Key Points:

- An extreme heat event along the southeastern coast of China was closely related to the outer circulation of Typhoon Lekima (2019)
- Upstream surface sensible heat flux, subsidence induced by Typhoon Lekima, and foehn effect due to local topography played approximately equal roles for the event
- Retreat of regional land-sea breeze circulation also favored the event

Supporting Information:

Supporting Information may be found in the online version of this article.

Correspondence to:

Y. Lin,
yanluan@tsinghua.edu.cn

Citation:

Zhao, D., Lin, Y., Li, Y., & Gao, X. (2021). An extreme heat event induced by Typhoon Lekima (2019) and its contributing factors. *Journal of Geophysical Research: Atmospheres*, 126, e2021JD034760. <https://doi.org/10.1029/2021JD034760>

Received 11 FEB 2021

Accepted 13 MAY 2021

An Extreme Heat Event Induced by Typhoon Lekima (2019) and Its Contributing Factors

Dingchi Zhao¹ , Yanluan Lin¹ , Yuanlong Li¹, and Xiaoyu Gao¹

¹Ministry of Education Key Laboratory for Earth System Modeling, Department of Earth System Science, Tsinghua University, Beijing, China

Abstract As two prominent natural hazards, tropical cyclone (TC) and heat compound events seem irrelevant on most occasions. TC generally leads to cooling, but could induce extreme heat days (EHD) and heat compound hazard under certain circumstances. An EHD along the southeastern coast of China (SECC) associated with Typhoon Lekima (2019) is documented with its major contributing factors. The formation and intensity of the EHD were found to be closely related to the outer circulation of Lekima by comparing a series of WRF simulations. Via a boundary layer heat budget, we found local sensible heat flux was a necessary, but not sufficient condition for this EHD. Aided by a backward trajectory analysis, we found that upstream surface sensible heat flux, subsidence induced by Typhoon Lekima, and foehn effect due to local topography played approximately equal roles to the occurrence of the EHD. The retreat of regional land-sea breeze circulation was also beneficial to the appearance of the EHD. Such TC-heat events might be more overwhelming due to more vigorous TCs with warming in the future.

Plain Language Summary Tropical cyclone (TC) and heat compound events pose a severe threat to human health and natural ecosystems. This paper documents an extreme heat days (EHD) along the southeastern coast of China associated with Typhoon Lekima (2019). Through a series of WRF simulations, we found that the formation and intensity of the EHD are closely related to the outer circulation of Lekima. The local sensible heat flux was necessary, but insufficient for the formation of the EHD. The upstream surface sensible heat flux, subsidence induced by Typhoon Lekima, and foehn effect due to local topography were the key factors to the occurrence of the EHD and the contributions of these three factors were approximately equal. Regional land-sea breeze circulation influenced by Lekima was also beneficial for the EHD. Such TC-heat events can be more widespread and severe due to increased intensity of tropical cyclones with warming.

1. Introduction

A combination of various extreme weathers may bring greater damages to human society and natural ecosystems than a single one of them (Zscheischler et al., 2018, 2020). Extreme heat days (EHD) that occur on both regional and global scales pose a severe threat to human beings (Meehl & Tebaldi, 2004; Mora et al., 2017). Destructive winds, torrential rain, and storm surge associated with tropical cyclones (TCs), often cause severe damage in coastal areas (Lin & Emanuel, 2016; Peduzzi et al., 2012). It seems that these two extreme weather types (EHD and TC) are isolated from each other because a coming TC would generally mitigate the drought and heat stress (Lam et al., 2012). However, TC-related heat compound events have been widespread and documented. For example, abnormal high temperature often occurs at the periphery of the spiral rainbands of TCs, before or during a TC's landfall (Chen et al., 2010; Parker et al., 2013; Shan & Meng, 2006; Shibata et al., 2010; Zhang et al., 2010). Note that extreme heat could be better measured using a product of air temperature and humidity (a metric to define humid heat) in the context of human comfort (e.g., Anderson et al., 2013; Sherwood & Huber, 2010). Matthews et al. (2019) showed the humid heat was unusually high before TCs landfall and highlighted the dangerous TC-heat compound events would become more likely under global warming. TCs also threat power supply when air conditioning was in high demand during TC-heat compound events (Lin, 2019). A better understanding of physical mechanisms underlying TC-heat compound events is critical for preparedness of such events and casualties mitigation.

EHD generally occurs under favorable large-scale and synoptic circulations. One common feature of synoptic systems in the EHD event is a high-pressure system (anticyclones) (Perkins, 2015). The western North

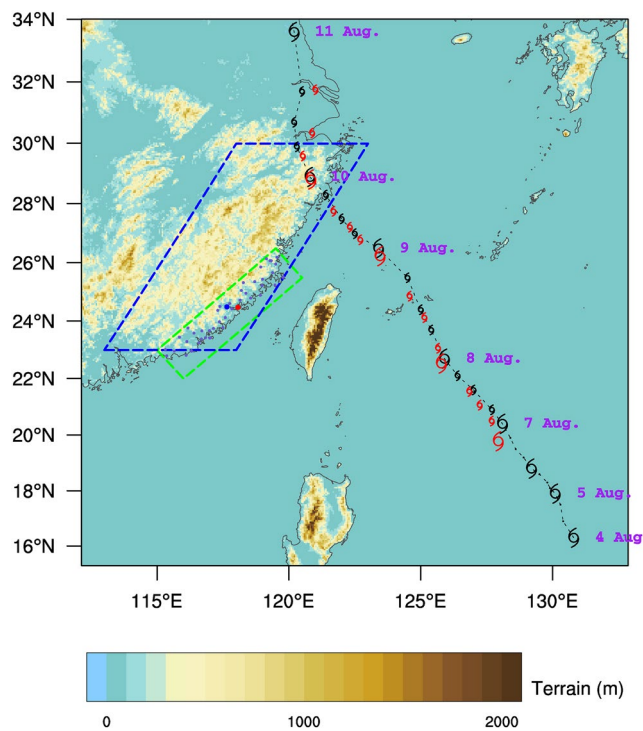


Figure 1. The domain configuration and topography for the WRF model overlaid with the track of Typhoon Lekima between 4 and 11 August 2019. Locations (cyclone symbols) and tracks (dash lines) of Lekima of best-track (black) and simulation (red) are shown for every day before 4–7 August 2019 and every 6 h between 0000 UTC 7–1800 UTC 10 August 2019. The dashed green box marks the region with extreme high temperatures. Solid dots within the green box denote the locations of meteorological stations. Red and blue solid dot denote Xiamen and Zhangzhou station. The dashed blue box marks the region where the terrain was removed in TOPO-EXP.

Pacific subtropical high (Chen & Lu, 2015; Chen, Wen, et al., 2019; Ding et al., 2010; Luo & Lau, 2017; Wang et al., 2016), East Asian Monsoon (Deng et al., 2020), and East Asian Jet Stream (Wang et al., 2016) are generally associated with the EHD in southeastern China in summer. TC activities have significant impacts on summertime synoptic circulations (Ahn & Lee, 2002; Arakane & Hsu, 2020; Chen, Zhong, et al., 2019; Hsu et al., 2008). The synoptic-scale circulation blocked by TCs can also lead to EHD. For example, Parker et al. (2013) found that the advection of anomalous anticyclonic potential vorticity from TCs' deep convection into the upper levels over Southeastern Australia played an important role in the development of severe heat days.

Favorable synoptic conditions cause and prolong an EHD event in three ways (Black et al., 2004; Fischer, 2014). The first is the strong solar radiation and land surface heat up under clear skies related to subsidence and dry environments (e.g., Black et al., 2004). The second is the continued adiabatic subsidence heating associated with a strong and stagnant anticyclone. Bieli et al. (2015) found that hot extremes in Balkans and UK were often driven by such an adiabatic descending compression. The third is related to advection of hot dry air to the region of interest. Miralles et al. (2014) found that the Mega-heatwaves in Europe were often supplied by large-scale horizontal advection. However, several studies (Bieli et al., 2015; Pfahl & Wernli, 2012) argued that the contribution of horizontal advection of warm dry air was small in midlatitude Europe since winds near the anticyclone were typically weak.

Besides favorable synoptic conditions, EHD could be induced by local adiabatic warming, such as foehn wind, commonly occurred in the lee of mountains with increased air temperature and decreased relative humidity due to adiabatic warming (Gaffin, 2007). Shibata et al. (2010) found that TCs could trigger foehn in the Hokuriku District of Japan during midsummer. Chen et al. (2010) analyzed the surface warming generated by TCs passing across Taiwan Island in downslope regions and revealed that the foehn effect was the major contributor to the surface warming. Yan et al. (2001) found a significant warming in the southeastern China

closely related to TC circulation and local topographic effect. Shan and Meng (2006) found that adiabatic warming due to strong subsidence in the outer perimeter of TCs was an important factor for the occurrence of the EHD in the Southeastern China in addition to the strong solar radiation.

Southeastern China is prone to TCs. Anomalous summer heat events in this area often occur with TCs approaching mainland China (Chen & Lu, 2015). The links between EHD in Southeastern China and TCs have been investigated by a number of studies (Huang et al., 2005; Ji et al., 2005; Shan & Meng, 2006). Zhong et al. (2019) analyzed the feedbacks between TCs and the western North Pacific subtropical high and found frequent TC activities could lead to more heat days in Eastern China. However, there are very few studies focused on the role of various physical processes and underlying mechanisms of TC-heat compound events in Southeastern China.

Record-breaking heat swept across the southeastern coast of China (SECC) region when Super Typhoon Lekima (2019) approached mainland China (Figure 1). This study aims to explore the dominant processes and mechanisms quantitatively for the formation of this EHD using numerical simulations. The paper is organized as follows. Data, numerical model setup, and various diagnostics are introduced in Section 2. The evolution and basic features of this TC-heat event are described in Section 3. Section 4 quantifies the contributions of Typhoon Lekima to the EHD using a series of numerical simulations. Summary and discussion are in Section 5.

Table 1
Summary of Numerical Experiments Performed in This Study

Experiment	Modifications
CTL	Control experiment
VR1-EXP	Remove the vortex of Lekima from the initial fields (including horizontal winds U, V, air temperature, SLP, water vapor mixing ratio, and geopotential height).
VR2-EXP	Remove the vortex of Lekima from the initial fields (only including horizontal winds U, V).
TOPO-EXP	Remove the terrain in southeast China all the time.

2. Data, Model Simulations, and Methods

2.1. Data

The best-track TC data was obtained from Shanghai Typhoon Institute, China Meteorological Administration (CMA), which included the 6-h location of the TC center, central sea level pressure (SLP) and maximum sustained (2-min mean) wind speed (Ying et al., 2014). Hourly observations of 2-m temperature (T2), daily maximum temperature (Tmax), precipitation and cloud cover at CMA meteorological stations were acquired from the China Meteorological Data Sharing Service System (<http://cdc.cma.gov.cn/home.do>). Data from the National Centers for Environmental Prediction Final operational global analysis (NCEP FNL) at $0.25^\circ \times 0.25^\circ$ horizontal resolution and 6-h intervals (<https://rda.ucar.edu/datasets/ds083.3/>) were also used in this study.

2.2. Model Setup

The WRF-ARW version 3.9 (Skamarock et al., 2008), a fully compressible, nonhydrostatic model, was used. WRF simulations covering part of Lekima's lifetime from 7–11 August 2019 were conducted using a daily re-initialization strategy (Dong et al., 2018). Specifically, simulations were conducted by integrating the model for 36 h starting at 1200 UTC each day. The first 12 h of the integration were discarded as model spin-up and the remaining 24 h were stitched together for a complete simulation over the period of interest. There were 35 uneven vertical levels with the model topped at 50 hPa. The center of the model domain was located at $(27^\circ\text{N}, 127^\circ\text{E})$ with a grid spacing of 2 km and 1000*1000 horizontal grid points. Both the initial and lateral boundary conditions were derived from NCEP FNL. The model physics used included Thompson microphysics scheme (Thompson et al., 2008), the Noah land surface model, the revised MM5 Monin-Obukhov surface layer scheme, the Yonsei University planetary boundary layer scheme (YSU_PBL) (Hong et al., 2006), and the RRTMG broadband model for longwave radiation and shortwave radiation (Iacono et al., 2008). No cumulus parameterization was used. The cloud fraction option selected for the simulation was Xu-Randall method (Xu & Randall, 1996). The 21-class MODIS land-use data was used (Friedl et al., 2010).

2.3. Sensitivity Experiments

To explore and quantify the connection between the EHD and Lekima, a series of experiments were conducted (Table 1). The control simulation (CTL) was performed using the settings described above. Two sensitivity experiments were conducted to demonstrate the influence of Typhoon Lekima on the extreme hot day in southeastern China. The first sensitivity experiment (VR1-EXP) was identical to CTL except that the vortex of Lekima, including its horizontal winds, air temperature, SLP, water vapor mixing ratio, and geopotential height, were removed from the initial conditions. In the second sensitivity experiment (VR2-EXP), only horizontal winds of the vortex of Lekima were removed from the initial conditions, while leaving other variables to be spun-up by the model itself, to ensure a weaker TC with a minimal position change. The vortex removal algorithm followed previous studies (Cha & Wang, 2013; Li et al., 2019; Zhang et al., 2019). To assess the impact of local terrain on the heat event, another experiment (TOPO-EXP), identical to the control, but with the terrain in southeast China (Figure 1) flattened, that is, with zero elevation during the integration, was also conducted.

2.4. Height Correction for Simulated 2-m Temperature

The terrain in the SECC region was complex, and the discrepancy of height between simulations and real terrain may lead to 2-m temperature (T₂) bias. Here, a height correction for temperature was conducted following Sheridan et al. (2010). Specifically, when compared with the station observation, the nearest grid was selected if its model height difference was less than 25 m. Otherwise, the point with the smallest height difference in the surrounding nine nearest grid points was selected. A height correction was applied after the model grid point was selected as $T_a = T_m + \gamma(h_m - h_a)$. Where T_a was the corrected simulated T₂ and h_a was the terrain height of station observations. T_m , h_m was the simulated T₂ and terrain height of selected grid point. The local value of lapse rate γ was obtained from the linear regression coefficient between the simulated T₂ and height variations within the 8*8 grid points nearest to the station observation.

2.5. Boundary Layer Heat Budget

To quantify the temperature variation associated with Typhoon Lekima, a spatially averaged boundary layer heat budget was conducted following Wang and Li (2019). The control volume for the budget covered the extreme heat box extending from the surface to the fifth sigma layer (detailed in Section 4.3). Assuming fixed air density and negligible evaporation, condensation and radiative flux divergence in the box, the boundary layer heat budget could be expressed as (detailed derivation of Equation 1 was in the supporting information):

$$\frac{\partial \bar{\theta}}{\partial t} = -\frac{\partial \overline{w' \theta'}}{\partial z} - \frac{\partial \bar{w} \bar{\theta}}{\partial z} - \frac{\partial \bar{u} \bar{\theta}}{\partial x} - \frac{\partial \bar{v} \bar{\theta}}{\partial y} \quad (1)$$

where θ was potential temperature, u , v , and w were wind speeds in longitudinal (x), lateral (y), and vertical (z) directions, respectively. The overbar indicated the temporal or spatial averages and the prime noted deviations from the average.

Equation 1 was integrated from the ground to the top of the boundary layer (about fifth sigma layer) over the control area A. Where z_i was the model height at the fifth sigma layer.

$$\int_0^{z_i} \int \frac{\partial \bar{\theta}}{\partial t} dz dA = \int_0^{z_i} \left(-\frac{\partial \overline{w' \theta'}}{\partial z} - \frac{\partial \bar{w} \bar{\theta}}{\partial z} - \frac{\partial \bar{u} \bar{\theta}}{\partial x} - \frac{\partial \bar{v} \bar{\theta}}{\partial y} \right) dz dA \quad (2)$$

Then Green's Theorem was used and both sides of Equation 2 were multiplied by $\frac{\rho c_p}{A}$, where ρ was the average density of control volume and c_p was the specific heat capacity of air.

$$\begin{aligned} \frac{\rho c_p}{A} \int_0^{z_i} \int \frac{\partial \bar{\theta}}{\partial t} dz dA &= \frac{\rho c_p}{A} \int \overline{w' \theta'}_{z=0} dA - \frac{\rho c_p}{A} \int \overline{w' \theta'}_{z=z_i} dA \\ &\quad - \frac{\rho c_p}{A} \int \bar{w} \bar{\theta}_{z=z_i} dA - \frac{\rho c_p}{A} \int_0^{z_i} \left(f(\bar{u} \bar{\theta}_e - \bar{u} \bar{\theta}_w) dy + (\bar{v} \bar{\theta}_n - \bar{v} \bar{\theta}_s) dx \right) dz \end{aligned} \quad (3)$$

where $\bar{u} \bar{\theta}_e$, $\bar{u} \bar{\theta}_w$, $\bar{v} \bar{\theta}_n$, and $\bar{v} \bar{\theta}_s$ were the products of the horizontal wind speed and the potential temperature at the east, west, north, and south surface of the control volume, respectively. The term on the left-hand side of Equation 3 indicated the average warming rate in the control volume. The terms on the right-hand side indicated the surface sensible heat flux, entrainment of heat flux at the boundary layer top, vertical heat flux through the top of boundary layer, and horizontal heat flux divergence, respectively. Among them, the surface sensible heat flux could be directly obtained from WRF output. Vertical and horizontal heat flux could be calculated from WRF output, where $\bar{w} \bar{\theta}_{z=z_i}$ was the products of the vertical wind speed and the potential temperature at the fifth sigma layer, $\bar{u} \bar{\theta}_e$, $\bar{u} \bar{\theta}_w$, $\bar{v} \bar{\theta}_n$, and $\bar{v} \bar{\theta}_s$ were the products of the horizontal wind speed and potential temperature at the east, west, north, and south surface of the control volume, respectively. The entrainment of heat flux was treated as residual errors together with some neglected physical processes

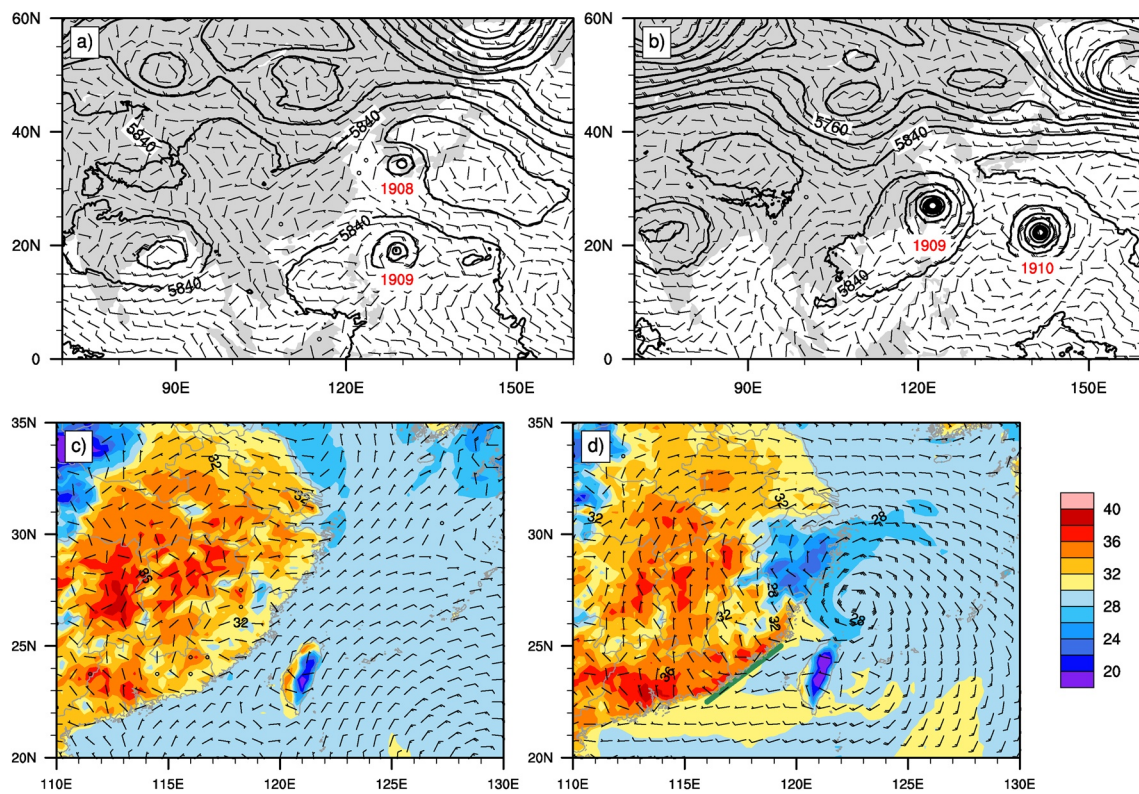


Figure 2. Synoptic features at 0600 UTC 6 August 2019 (a), (c) and 0600 UTC 9 August 2019 (b), (d). (a)–(b) Distribution of geopotential height (shading, units: gpm) and wind (vectors, units: m/s) at 500-hPa. The red number indicates the typhoon number, 1908 for Typhoon Francisco, 1909 for Typhoon Lekima, 1910 for Typhoon Krosa. (c)–(d) Distribution of 2-m temperature (shading, units: °C) and 10-m winds (1 full barb is 10 kt). The green solid line in (d) indicates the convergence line between the northwesterly and southwesterly.

(e.g., evaporation, condensation and radiative flux divergences) and numerical errors. Vertical velocity w was calculated by mass conservation, namely the subsidence had to balance the horizontal divergence.

3. Evolution of the EHD

3.1. Synoptic-Scale Evolution

The synoptic pattern from upper-level to surface was described based on FNL reanalysis. At 200 hPa level (not shown), alternating troughs and ridges propagated along the East Asian upper tropospheric westerly jet stream. A saddle pattern persisted over Southeastern China at 500 hPa (Figures 2a and 2b). On 6 August 2019, a trough moved across 110°E to affect eastern China (Figure 2a). Convective clouds appeared in southeastern China in the afternoon (Figure S1), but no EHD was detected over the SECC region. Another trough approached near 110°E (Figure 2b) on 9 August 2019. At this time typhoon Lekima approached China mainland with its center over the East China Sea (122°E, 27°N) and its upper level outflow started to be partly responsible for the EHD over the SECC region (Figure S2). The EHD started to form under a prominent upper-level (approximately 200 hPa) convergence associated with the outflow from Lekima, which favored the observed deep subsidence extending from 200 to 700 hPa (Figure S3). The large relative humidity (RH) contrast crossing 700 hPa from the radiosonde profile also supported the existence of deep subsidence (Figure S4).

Near surface (Figures 2c and 2d), on 6 August 2019, northeasterly prevailed over the Taiwan Strait, and the SECC region was cool and humid due to the presence of regular sea breeze. On 9 August 2019, due to the circulation of Lekima, wind shifted to southwesterly over the Taiwan Strait with northwesterly over the SECC region, which brought hot and dry air from the inner land to the SECC region. With the retreat

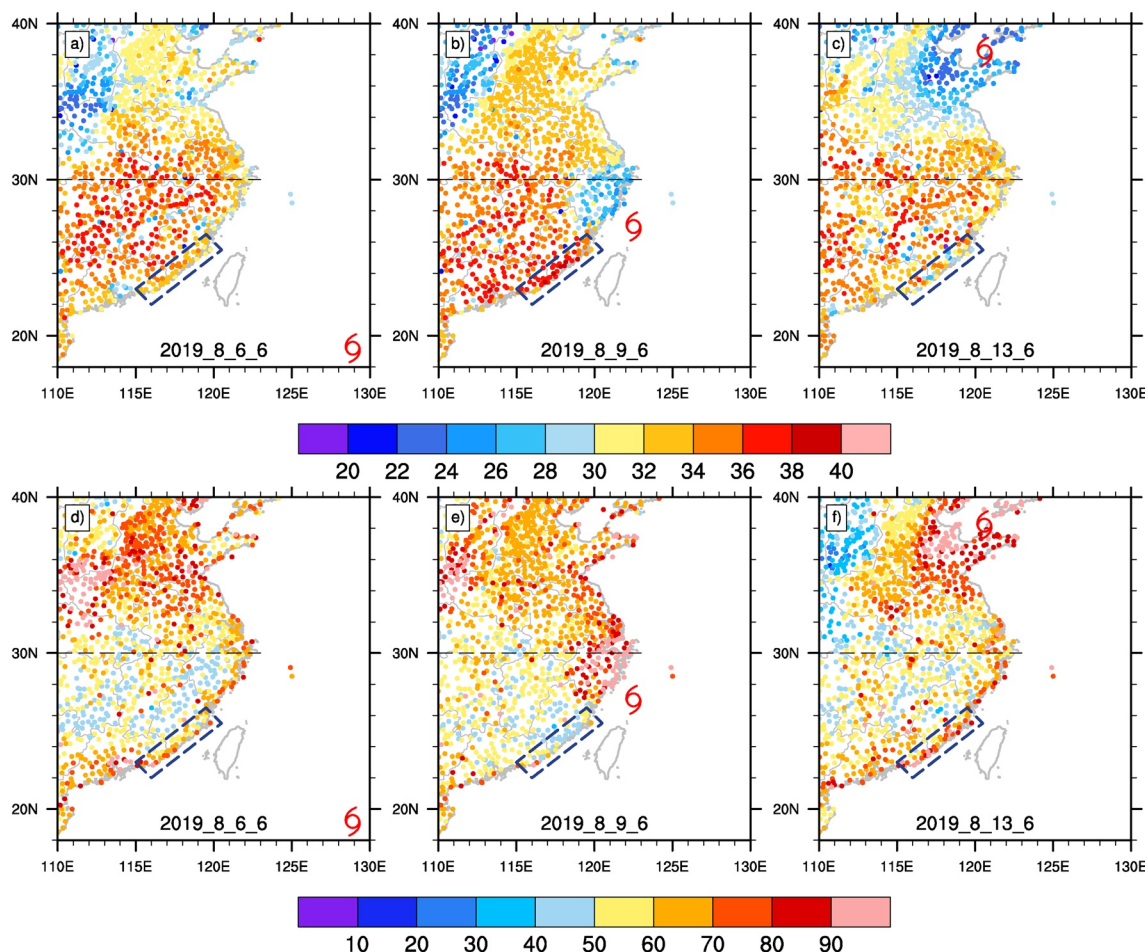


Figure 3. Distribution of surface air temperature (a, b, c, units: °C) and surface relative humidity (d, e, f, units: %) at meteorological stations before (a), (d), during (b), (e) and after (c), (f) Lekima approaching the Chinese mainland. The dashed navy-blue rectangle marks the extreme high temperatures area. South of the dashed black line denoted the southeastern China.

of land-sea breeze, a convergence line formed between the SECC region and the Taiwan Strait (green solid line in Figure 2d). The EHD event occurred to the west of the convergence line and the subsidence above 700 hPa might have inhibited this convergence from precipitation formation.

3.2. Typhoon Lekima and the Concurrent EHD

Typhoon Lekima originated and developed gradually east of the Philippines on 4 August 2019. At 0600 UTC (1400 LST) 6 August 2019, when Typhoon Lekima was located at about 1,000 km southeast of Taiwan Island (Figures 3a and 3d)), surface temperatures were above 35 °C with RH below 50% at most stations in southeastern China (south of 30°N and east of 110°E as indicated in Figure 3). The SECC region was generally cooler and moister than the interior land area due to the regular sea breeze and moisture transport from the Taiwan strait. Lekima reached its peak intensity on 8 August 2019, with a maximum sustained wind speed of 62 m/s and a minimum central SLP of 915 hPa in the East China Sea. As Lekima approached the coast of Chinese mainland (Figures 3b and 3e), many stations along the southeastern coast recorded extreme high temperatures and low humidity at 0600 UTC 9 August 2019. A new surface temperature record (39.6°C) was measured at Xiamen (red solid dot in Figure 1), a coastal city in Fujian Province since the station was established in 1953. Forty of the 41 stations in the SECC region measured daily maximum temperatures above 35°C. On the other hand, surface temperatures in Zhejiang province were lower than 30°C with RH above 80% because of the outer spiral rainbands of Typhoon Lekima (not shown).

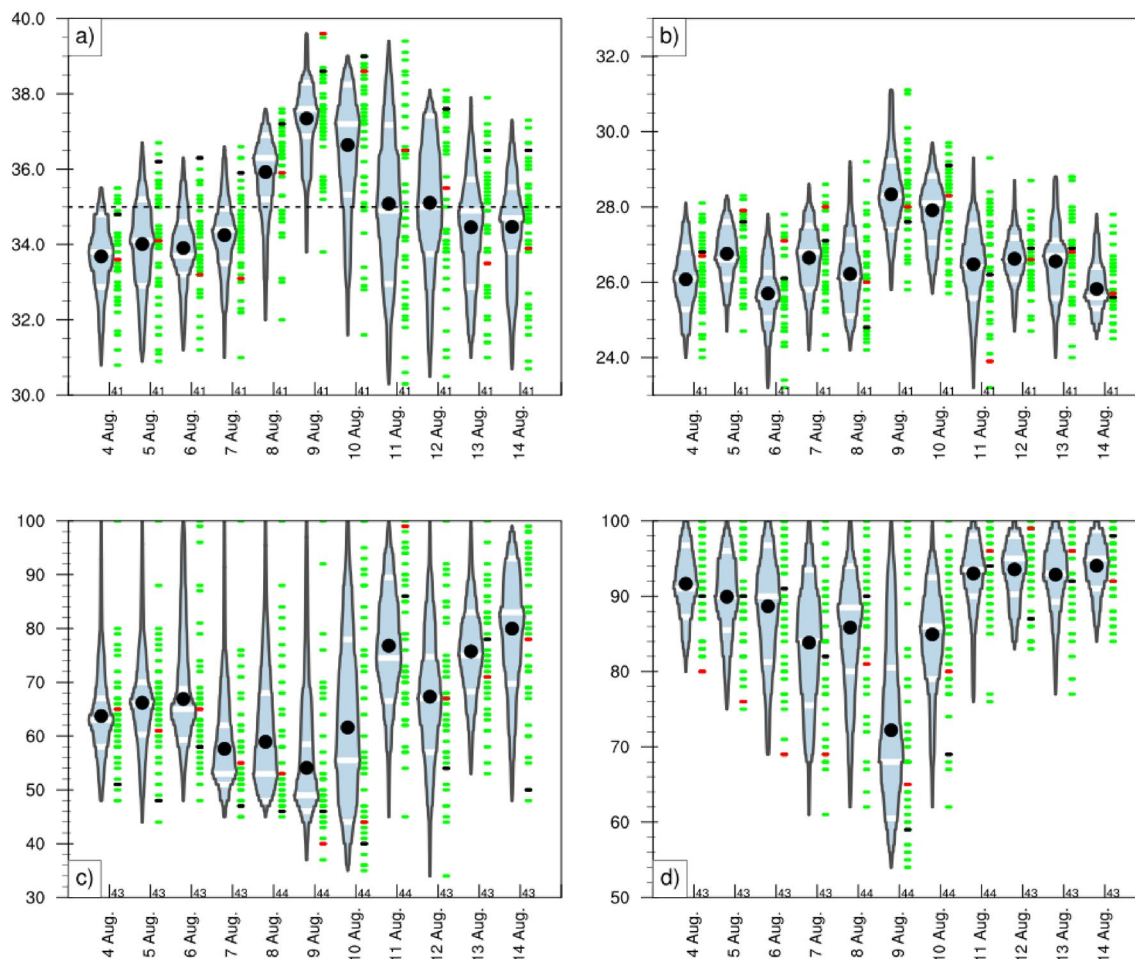


Figure 4. Daily maximum temperature (a), daily minimum temperature (b), relative humidity at 0800 UTC (c), and relative humidity at 2000 UTC (d) at meteorological stations in the SECC region during the lifetime of Lekima. The black solid dots in the box plot indicate mean values. The white short dashes in the box plot indicate the 25th, 50th, and 75th percentiles from the bottom up. The red, black, and green short dashes on the right of box plot indicate Xiamen, Zhangzhou, and other sample values. The numbers below each box plot represent the number of measurements. Extreme heat days at specific stations are identified by daily maximum temperature exceeded 35°C, which is commonly used by the CMA.

Between 1500 and 1800 UTC on 9 August, the typhoon made landfall at Wenling, Zhejiang Province (c.f. Figure 1) with a maximum sustained wind speed of 52 m/s and a minimum central SLP of 930 hPa. Thereafter, Lekima moved into the Yellow Sea on 11 August before making a second landfall at Qingdao, Shandong Province on the same day, and then crossed the Shandong Peninsula into the Bohai Sea, where it recurved and gradually dissipated on 14 August (not shown). As a result, the extreme high temperature and low humidity in SECC region disappeared (c.f. Figures 3c and 3f) when Lekima moved northward and weakened gradually.

Figures 4a and 4b show the evolution of daily maximum and minimum surface air temperature in the SECC region during the lifetime of Lekima. The average daily maximum temperatures in the study area were between 33.5°C and 35°C during the lifetime of Lekima except for 8–10 August. On 9 August, the average daily maximum temperature in the SECC area reached 37.50°C (Figure 4a). The average daily minimum temperatures in the study area were between 25°C and 27°C during the lifetime of Lekima except for 9–10 August. It was a very hot night on 9 August and the minimum temperature at 40 of the 41 stations in SECC exceeded 26°C with one above 30°C. RH at 0800 UTC (1600 LST) and 2000 UTC (0400 LST), roughly at the time of daily maximum and minimum surface air temperature, were shown in Figures 4c and 4d. The average RH in this area reached a minimum of 54.1% at 0800 UTC on 9 August. It increased to 72.2% at 2000 UTC on 9 August, which was the only day with average RH below 83% during the lifetime of Lekima.

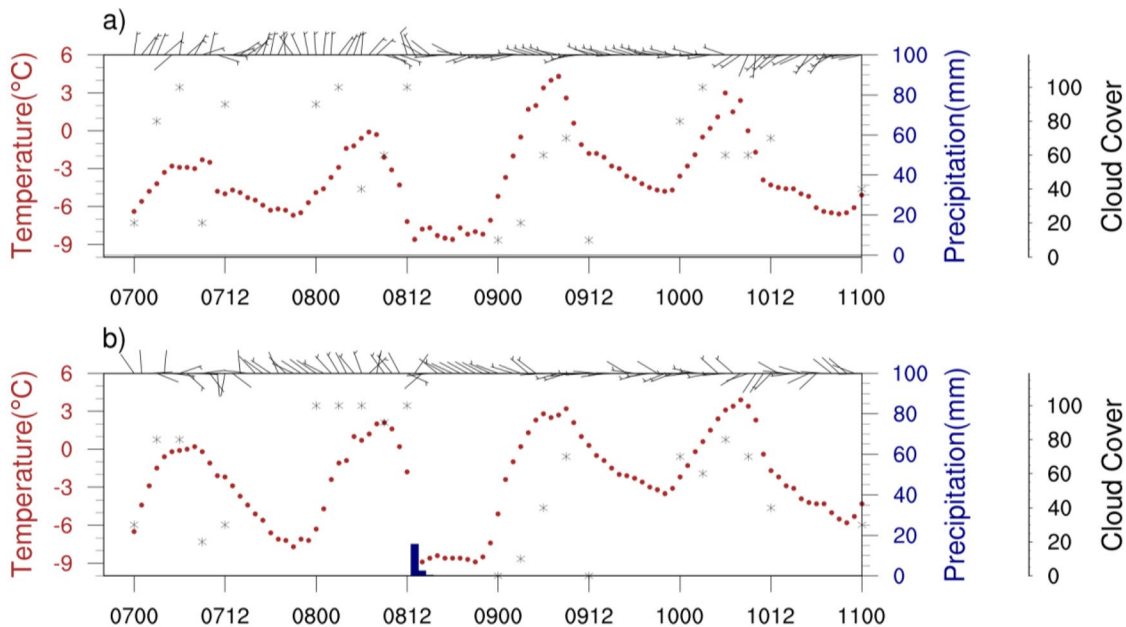


Figure 5. Evolution of hourly surface air temperature (labeled as deviations relative to 35°C, brown points, units: °C), hourly precipitation (blue histograms, units: mm), cloud cover (gray stars, every 3 h, units: %), and winds (wind barbs, every 3 h, full-wind barbs correspond to 10 kt) during the lifetime of Lekima at Xiamen (a) and Zhangzhou (b).

The highest temperature in the EHD event was recorded at Xiamen, followed by Zhangzhou nearby. The evolution of hourly maximum surface air temperature, precipitation, cloud cover and winds during 4–14 August at the two stations are shown in Figure 5. Both stations had less cloud cover on 9 August than other days. Xiamen had no precipitation for more than 6 days. These conditions favor a gradual increase of temperature. Before 1200 UTC 7 August, Xiamen and Zhangzhou stations were mainly dominated by northeast winds, and shifted to the southeast in the afternoon because of the sea breeze (see wind barb in Figure 5). Due to the influence of Lekima, wind shifted to northerly on 8 August and then shifted to westerly in the early morning of 9 August at both sites. After Lekima made landfall, the westerly at both stations changed to southwesterly. The high temperatures in the SECC area occurred in the afternoon of 9 August.

The above observational analysis indicated that the EHD was closely related to Typhoon Lekima, but the underlying mechanisms behind this TC-heat event are not clear. We conducted a series of numerical simulations for further exploration.

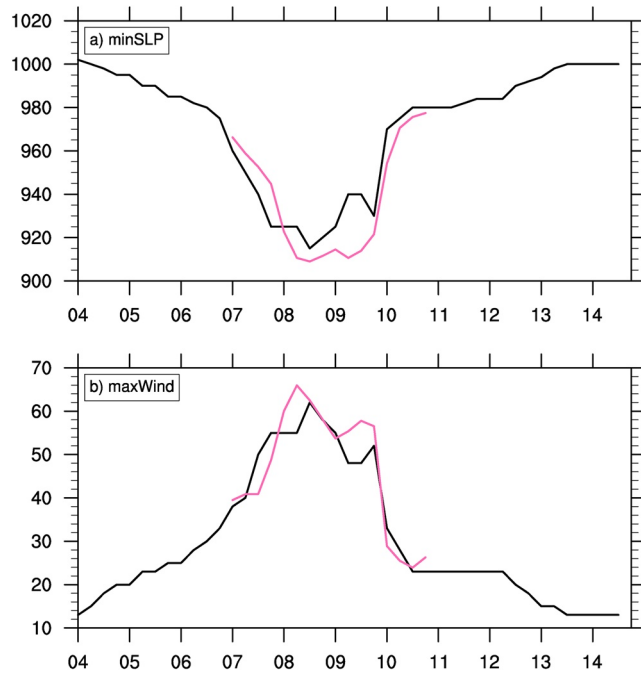


Figure 6. The 6-hourly central SLP (a, units: hPa) and 10-m maximum sustained wind speed (b, units: m s⁻¹) of Typhoon Lekima from the best-track data (black line) and the control simulation (CTL, pink line) between 4 and 14 August 2019.

4. Simulation Results

4.1. Control Simulation Evaluation

WRF model was used to simulate the TC-heat event with the detailed configuration shown in Section 2.2. Both the track (Figure 1) and intensity (Figure 6) of Lekima were reasonably reproduced in the CTL simulation as compared to the best-track data. The average track bias was about 52 km. The simulated location of the typhoon center at 0600 UTC on 9 August, when the EHD occurred in the SECC region, was about 32 km southeast of the observation. The average bias of intensity was

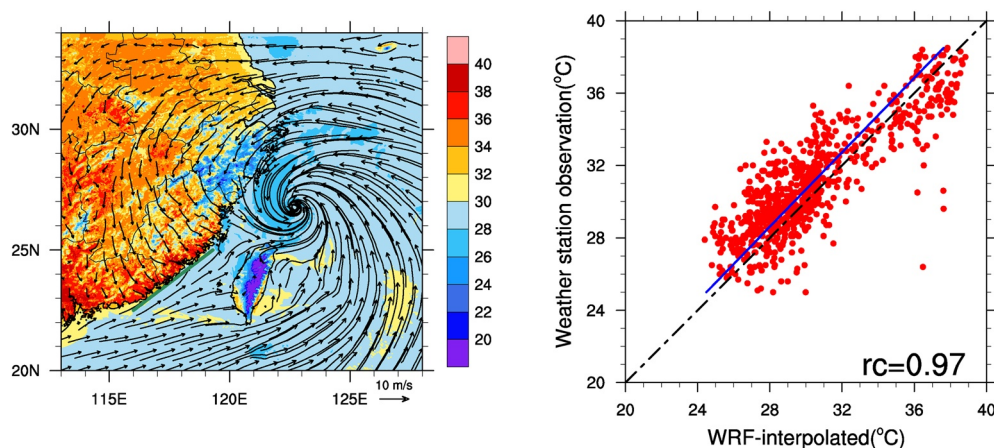


Figure 7. Left panel is the distribution of 2-m temperature (shading, units: °C) and surface circulation (streamline) at 0600 UTC 9 August 2019. The green solid line indicates the convergence line between the northwesterly and southwesterly. Right panel is the scatterplot of station-observed temperatures and those from CTL over SECC region every 6 h from 0000 UTC 7 August to 0000 UTC 11 August 2019. An elevation correction of simulated T2 has been done before comparing with observations.

about 4.1 m/s for the maximum 10-m wind speed and about 11.2 hPa for the minimum sea level pressure throughout the simulation (Figure 6).

The WRF simulation also successfully reproduced the spatial distribution and temporal variation of temperatures in the SECC region. Simulated T2 (Figure 7a) had a similar spatial distribution as observations at 0600 UTC 9 August 2019 (Figure 3b). Low temperature appeared in Zhejiang Province due to the precipitation effect of the spiral rain belt around the typhoon. Temperatures in other areas south of 30°N were relatively high, and extreme high temperatures appeared in the SECC region. A convergence line between the northwesterly dominated by the circulation of Typhoon Lekima and the southwesterly in the Taiwan Strait appeared along the coast of China mainland (the green solid line in Figure 7a). The correlation coefficient between the simulated and observed T2 at stations in the SCEE region reached 0.97 (Figure 7b). The diurnal variations of T2, RH, and wind were also well reproduced (Figure 8). The average wind direction of stations in SECC shifted from northeasterly to westerly with wind speed increased notably in the afternoon of 9 August. The appearance of maximum temperature on August 9 in the SECC was captured, although slightly overestimated. There were small cold and wet biases at night with overestimated wind speeds partly related to the complex terrain along the coast. Overall, the simulation of both Typhoon Lekima and the EHD event were in good agreement with observations, giving confidence to the following analyses. The following analysis focused on the daytime warming process.

4.2. Sensitivity Simulations

To quantify the connection between the EHD and TC, a series of experiments was conducted (Table 1). In VR1-EXP, Typhoon Lekima almost disappeared and the strong northwesterly along the SECC region weakened significantly compared with CTL (Figure 9a). The most significant difference in T2 between VR1-EXP and CTL was the higher T2 in VR1-EXP in Zhejiang Province and north of Taiwan Island, due to significantly decreased typhoon precipitation (Figure 9d). Most points along the SECC region were 2–6°C cooler in VR1-EXP than CTL and some points in the south part within the rectangle were more than 8°C cooler than CTL partly due to the precipitation in VR1-EXP. Therefore, without Typhoon Lekima, the EHD in the SECC region would not have occurred.

Compared to CTL, the center of the TC was similar in the East China Sea north of Taiwan Island, but the intensity decreases in VR2-EXP. The SECC region was still controlled by the north-to-northwest wind outside the typhoon, but the wind speed was significantly reduced (Figure 9b). Most points along the SECC region in VR2-EXP were 0–4°C cooler than CTL (Figure 9e), which meant the severity of EHD was related to the intensity of the typhoon. T2 along the SECC region in VR2-EXP was overall higher than that in VR1-EXP,

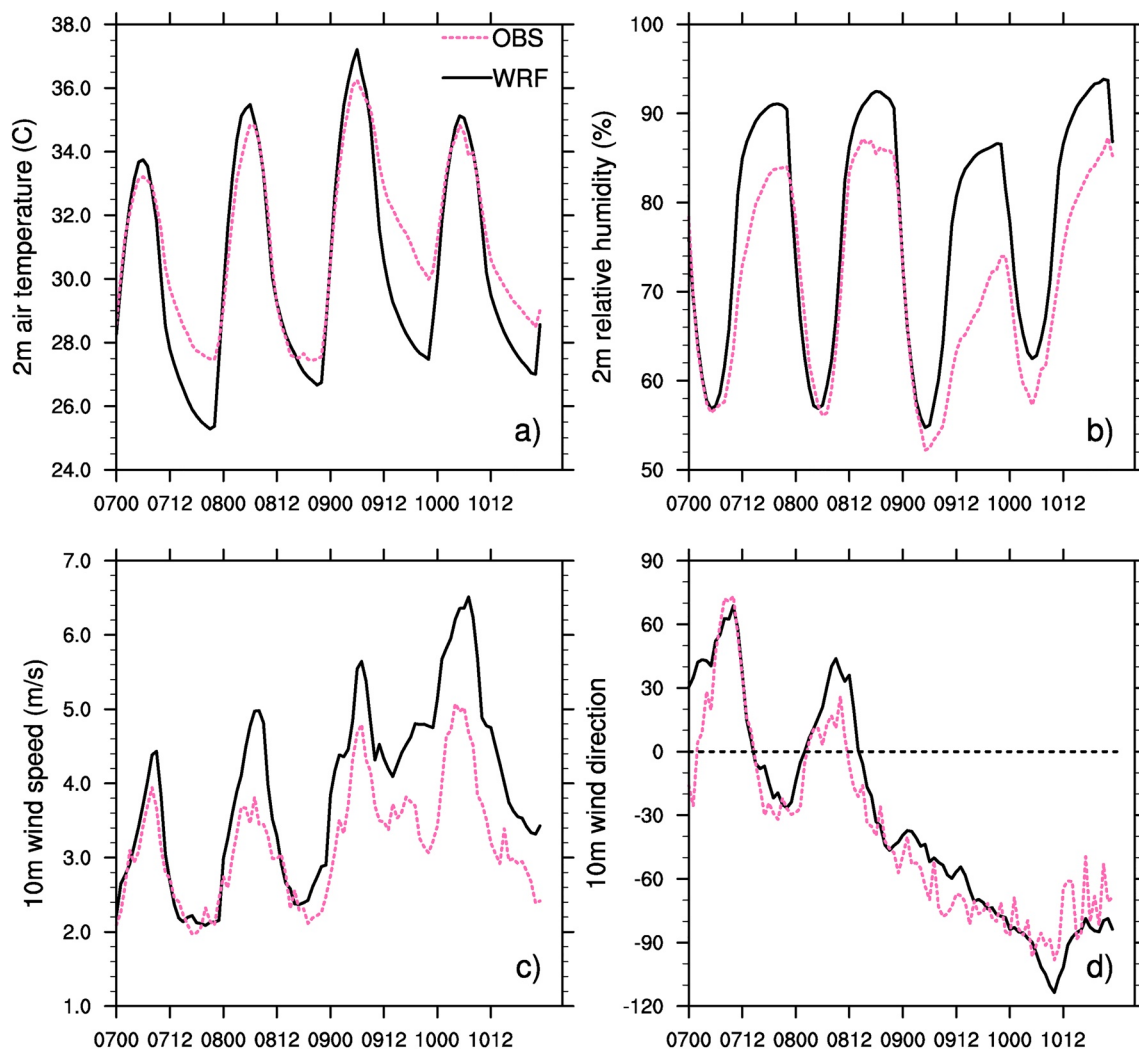


Figure 8. Diurnal variations of the averaged T2 (a), 2 m relative humidity (b), 10 m wind speed (c), and 10 m wind direction (d) in the SECC region from 0000 UTC 7 August to 0000 UTC 11 August 2019. The pink dash line represents the average of station observations in the SECC region. The black solid line represents the average of simulated results with height correction in the SECC region from the CTL.

in which the north part of SECC region was dominated by northeasterly and the south part was dominated by southeasterly. It meant that westerly winds from inland might be more conducive to the warming event than easterly winds from the Taiwan Strait.

Although the track and intensity of Typhoon Lekima in TOPO-EXP differ negligibly from CTL (Figure 9c), T2 in southeast China was higher in TOPO-EXP than CTL (Figure 9f). Some points in the north of the moved terrain area were more than 8°C warmer in TOPO-EXP than CTL because of the lowered elevation. T2 near the coastline area was about 2–6°C cooler in TOPO-EXP than CTL. This suggests that topography, that is, the foehn wind effect, also contributes significantly to the EHD event.

Figure 10 shows the time series of T2 from all the simulations at Xiamen. Temperature evolution was well captured by the CTL at Xiamen, with the maximum of 37.4°C, slightly lower than the observed 39.30°C at 0800 UTC (1600 LST). Temperature in VR1-EXP, VR2-EXP, and TOPO-EXP simulations at 0800 UTC were 30.6°C, 32.7°C, and 35.7°C, respectively. This suggests that both typhoon and local topography are critical for the EHD. The simulated temperature in VR1-EXP and VR2-EXP reached its maximum at 0500 UTC (1300 LST) and 0600 UTC (1400 LST), 3 and 2 h earlier than observed. This meant that horizontal heat transport after the time of peak solar radiation might also contribute to the EHD.

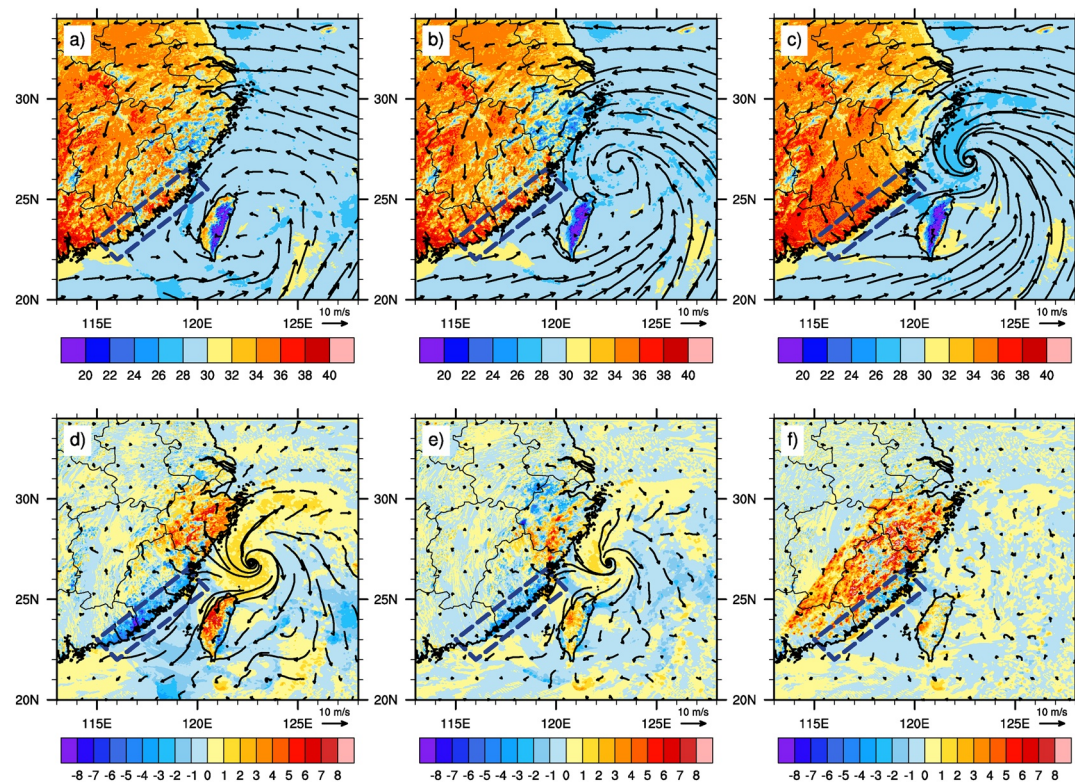


Figure 9. Distribution (a, b, c) and difference with CTL (d, e, f, EXP-CTL) of T2 (shading, units: $^{\circ}\text{C}$) and 10-m wind (vectors, units: m/s) at 0600 UTC 9 August 2019 in VR1-EXP (a), (d), VR2-EXP (b), (e), and TOPO-EXP (c), (f).

4.3. Boundary Layer Heat Budget

Not only surface temperatures, but also temperatures in the planetary boundary layer (PBL) in the SECC region on 9 August in CTL were significantly higher than those at other times and in other experiments (Figure 11). The PBL exhibited a pronounced diurnal cycle due to the alternating heating and cooling of ground surface. The temperature increase in the morning of ninth in CTL were greater and the static stability ($\partial\theta / \partial z$) were less than other simulations. The heat budget (detailed in Section 2.5) was conducted over a control volume covering a region with 7*8 original WRF horizontal grid points over Xiamen. Given that Xiamen is an island, the selected region was small in order to exclude the influence of land-sea surface contrast. Surface sensible heat fluxes were similar (approximately 300 W/m^2) before and after Typhoon Lekima in all experiments (Figure 12). This implied that local radiation or sensible heat flux from the surface was

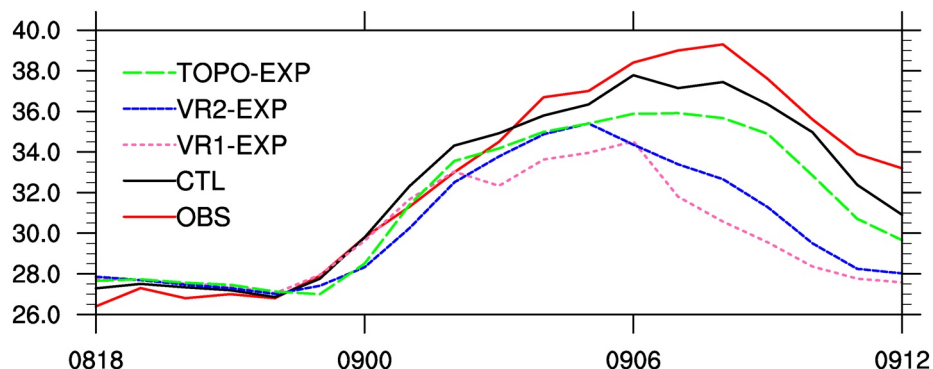


Figure 10. The time series of average 2-m temperature (units: $^{\circ}\text{C}$) at Xiamen station (in the GMT+8 Time Zone).

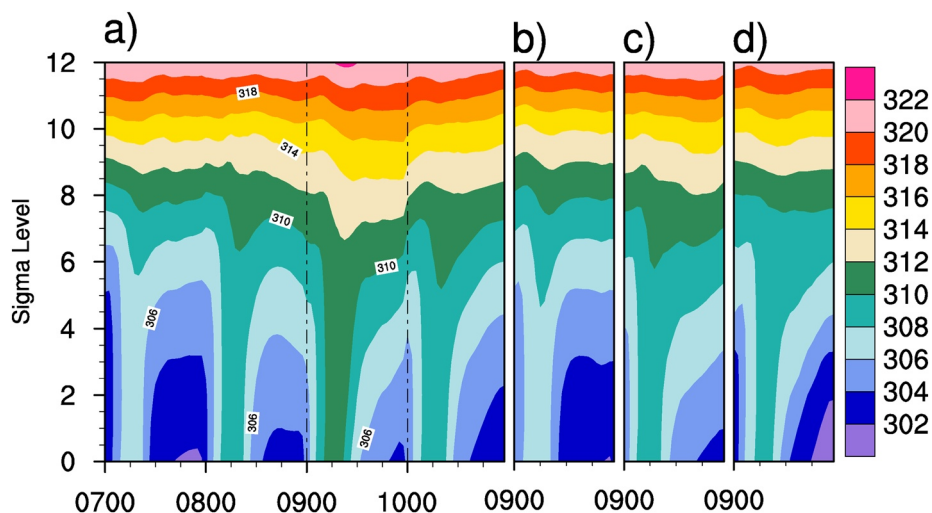


Figure 11. Vertical profiles of average potential temperature (units: K) from sigma level 0 to 12 (at approximately 3,800 m) in the SECC region from 7 to 11 August 2019 in CTL (a) and from 9 to 10 August 2019 in VR1-EXP (b), VR2-EXP (c), and TOPO-EXP (d). The black dash lines in (a) represent the EHD period.

a necessary, but not a sufficient condition for the EHD event. In Xiamen area, the positive heat transport term (including vertical and horizontal heat flux) in the late morning and early afternoon on 9 August led to a larger warming rate (Figure 12a), coincident with the onset of high temperatures. In VR1-EXP, the heat transport was negative in the daytime (Figure 12b) due to cooler air advected from the Taiwan Strait and residual term was negative due to low level rain evaporation (Figure S5). Similar to VR1-EXP, the heat transport was negative in VR2-EXP with a small residual term (Figure 12c). In TOPO-EXP, the surface sensible heat flux was slightly smaller than others with a small residual term, and the heat transport was negative in the afternoon (Figure 12d). These results suggest that the heat transport (including vertical and horizontal heat flux) is a key for the occurrence of the EHD.

4.4. Backward Trajectory Analysis

The upstream heat transport to Xiamen is characterized by a temperature increase due to subsidence (adiabatic heating) and surface sensible heat flux (diabatic heating). In order to distinguish the contribution of these two paths and the contribution of local foehn wind, we used a Lagrangian backward trajectory analysis extending 20 h before the extreme temperature in Xiamen area (Sprenger & Wernli, 2015; Takane & Kusaka, 2011; Takane et al., 2015; Wernli & Davies, 1997) by analyzing the dry static energy (s ; J/kg)

$$s = c_p T + g z. \quad (4)$$

Here, $c_p T$ was the sensible heat energy and gz was the geopotential energy. Generally, diabatic heating included surface sensible heat flux, condensation, and radiation. In this event, condensation and radiative heating were relatively small. Considering that Zhangzhou Station stood in the upstream of Xiamen Station and might have an impact on temperature variation of Xiamen, the backward trajectory analysis was also conducted for Zhangzhou area (covering 15*12 original WRF horizontal grid points).

In Xiamen area, according to the direction of the incoming air parcels, air parcels' trajectories could be divided into a southwest course and a west course. The southwest course consists of about 35.7% of all the 56 air parcels, while the west course consisted of the remaining 64.3% (Figure 13). The mean temperature of the air parcels in the west and southwest course at 0800 UTC 9 was 38.0°C and 34.8°C. It indicated that the influence of typhoon on sea breeze circulation was beneficial to the appearance of the EHD in the SECC region. In addition, the location of the EHD corresponded well to the horizontal convergence between the northwesterly and southwesterly, which is conducive to the accumulation of warm air in the SECC region (Figure S6).

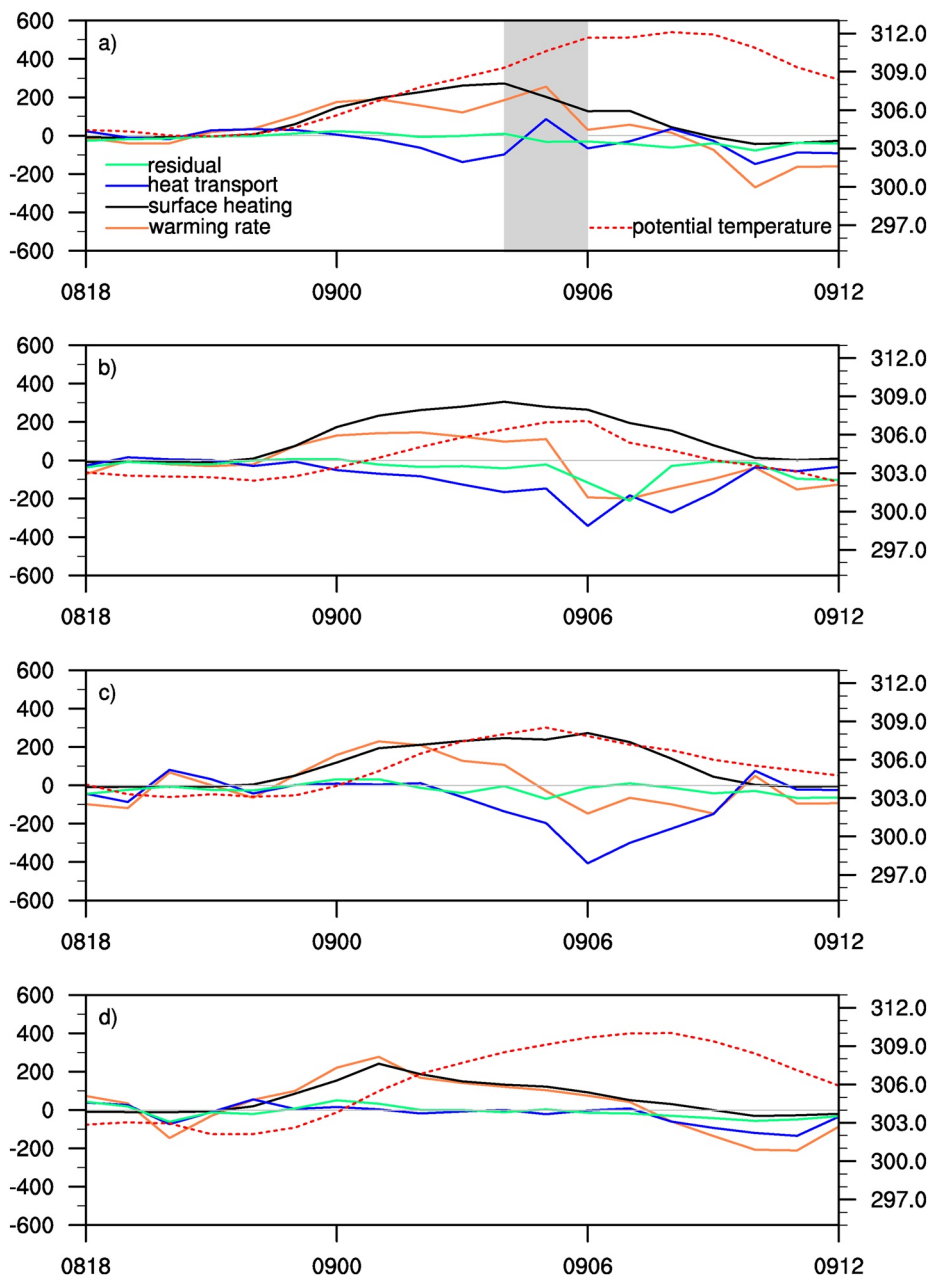


Figure 12. Temporal changes of the warming rate, the surface sensible heat flux, heat transport (horizontal advection and corrected subsidence) and the residual term (units: W m⁻², left-hand axis) and potential temperature in K (red dotted line using the right-hand axis) from 1800 UTC 8 to 1200 UTC 9 August at Xiamen from CTL (a), VP1-EXP (b), VP2-EXP (c), and TOPO-EXP (d). The translucent gray rectangles in (a) denote the period with positive heat transport.

In Zhangzhou area, 330 air parcels (every grid was an air parcel) were tracked backward every 10 min from 0800 UTC 9 to 1200 UTC 8 from the lowest level of the model grids using wind components of u, v, and w. All air parcels moved counterclockwise along the outer circulation of the typhoon (Figure 14). According to the height of the trajectory, air parcels could be roughly divided into an upper course and a lower course. The upper course consists of about 41% of all the trajectories and the height of these trajectories is great than 2,000 m (Figure 14b). The lower course consists of about 59% of all the trajectories with height below 2,000 m (Figure 14c).

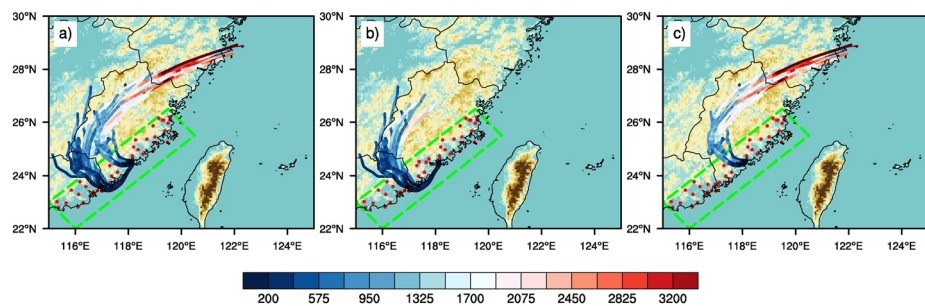


Figure 13. Backward trajectories of parcels of (a) all trajectories, (b) southwest-course trajectories (about 35.7%) and (c) west-course trajectories (about 64.3%) in Xiamen area. The color indicates the height (units: m) of trajectories.

The Lagrangian mean energy budget along the trajectories for the upper and lower course was shown in Figure 15. In the upper course (Figure 15a), s remained almost constant except for a slight decrease before 0200 UTC 9 August and a slight increase between 0200 UTC and 0500 UTC due to surface sensible heat flux. The increased sensible heat energy $c_p T$ relied mainly on upstream adiabatic subsidence (associated with decreased geopotential energy gz). Air parcels started to descend since 1200 UTC 8 August due to typhoon-induced subsidence, followed by a rapid descent due to local foehn wind after 0500 UTC 9 August. That is, the upper course air parcel temperature change was mainly contributed by subsidence and local foehn wind. In the lower course (Figure 15b), the sensible heat energy $c_p T$ remained almost constant until 0000 UTC 9 August. It increased initially due to upstream sensible heat flux and later due to local foehn wind after 0000 UTC 9 August. That is, the lower course air parcel temperature change was mainly contributed by upstream sensible heat flux and local foehn wind. The average temperature of the air parcels of the upper and lower course at 0800 UTC (1600 LST) were 37.1°C and 36.7°C, respectively. It indicated that the subsidence and upstream sensible heat flux had comparable contributions with the local foehn effect.

The upstream sensible heat flux and foehn wind warming contributions in the lower course was compared in Figure 15b. A diabatic warming (upstream sensible heat flux warming) of 6.27°C was slightly lower than adiabatic warming (foehn effect) of 7.02°C. The anomalous upstream sensible heat flux was due to the large upstream insolation (not shown) and the long journey of boundary layer air parcels (Figure 14c). The warming from the foehn wind and surface sensible heat flux was approximately equal in the lower course. In summary, adiabatic subsidence warming induced by the typhoon and foehn wind, and surface sensible heat flux were the three main causes (roughly equal based on the energy budget) for the warmed air parcels in Zhangzhou area.

In TOPO-EXP, temperature in Zhangzhou area was 35.03°C in the upper course and 35.15°C in the lower course (Figures S7-S8), which was about 2°C lower than CTL due to the missed foehn effect. It also suggested that the contribution of sensible heat flux from upstream surface and subsidence induced by Typhoon Lekima are similar.

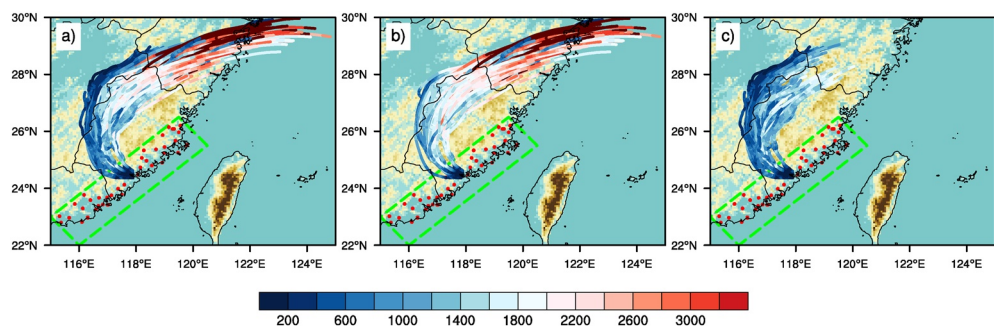


Figure 14. Backward trajectories of (a) all trajectories, (b) high-course trajectories (above 2,000 m, about 41%), and (c) low-course trajectories (below 2,000 m, about 59%) in Zhangzhou area. The color indicates the height (units: m) of trajectories.

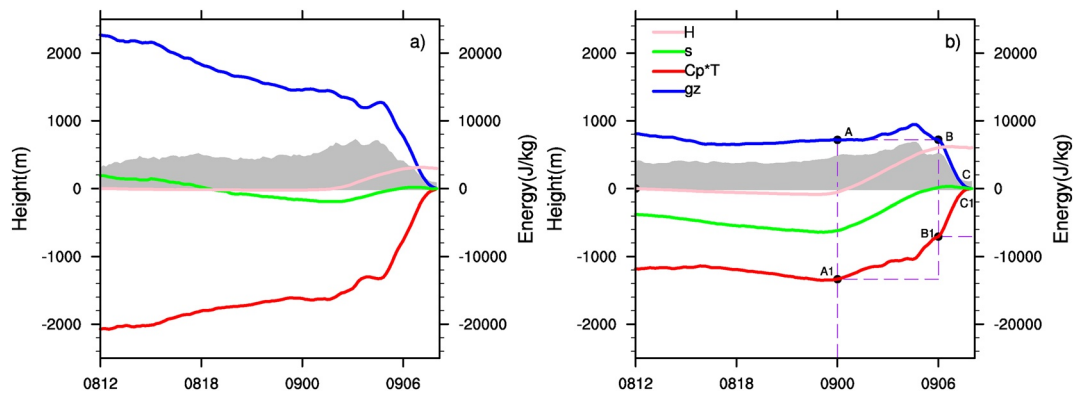


Figure 15. The mean energy variation (J kg^{-1}). The left y axis indicated the terrain height and the right y axis indicated averaged energy (J kg^{-1}) along the trajectories for the high course (a) and the low course (b). The blue, red, green line indicates the geopotential energy g_z , sensible heat energy $C_p T$ and dry static energy s , respectively. All are deviations relative to that at 0800 UTC 9 August 2019. The pink line shows the time-integrated sensible heat flux (H). Gray Shading is the terrain heights along the trajectories. In (b), A and A1 indicated the g_Z and $c_p T$ at 0000 UTC August 9. C and C1 indicated the g_Z and $c_p T$ at 0800 UTC August 9. g_Z at B was equal to A, which meant that the temperature increased between A1 and B1 was due to diabatic warming, that is, the sensible heat flux from surface of inner land (upstream). The temperature increased between B' and C' was due to adiabatic warming, that is, the local foehn wind due to the decreased terrain height toward the coast. The mean temperature at A', B', and C' was 23.45°C , 29.72°C , and 36.74°C , respectively. The diabatic warming (6.27°C) was slightly lower than adiabatic warming (7.02°C).

5. Discussion and Conclusions

As Typhoon Lekima approached Chinese mainland, the SECC region experienced an EHD. To systematically investigate the connection between Typhoon Lekima and the EHD and associated mechanisms, we analyzed the synoptic-scale and local-scale evolution of the TC-heat event using a series of WRF numerical simulations. Our findings are summarized as follows:

- (i) Diurnal variation of temperature in the boundary layer was mainly regulated by the local surface sensible heat flux, but it is not sufficient to explain the occurrence of the EHD in the SECC region.
- (ii) Upstream heat transport, including upstream surface sensible heat flux, subsidence induced by Typhoon Lekima, and foehn effect due to local topography, were the three key factors to the occurrence of the EHD. The contributions of these three factors were roughly equal (Figure 16).
- (iii) The influence of typhoon on land-sea breeze circulation was beneficial to the appearance of the EHD in the SECC region. In Xiamen area, air parcels coming along the coastline were 3.2°C cooler than that from inland. Horizontal convergence between the northwesterly and southwesterly help the accumulation of warm air in the SECC region.
- (iv) The strength of heat transport and foehn wind was closely related to the intensity of typhoon simulated.

Previous studies had noted the relationship between Typhoon and EHD event in the SECC region, but most of them only qualitatively discussed the links between EHD in Southeastern China and TCs (Huang et al., 2005; Ji et al., 2005; Yan et al., 2001) without a detailed analysis of underlying mechanisms. Shan and Meng (2006) considered that subsidence induced by typhoon was an important factor for the occurrence of EHD. Zhang et al. (2010) argued that warm advection contributed more than typhoon induced subsidence. In this study, we systematically investigated the effects of local and upstream surface sensible heat flux, subsidence induced by typhoon, foehn effect, and local land-sea breeze circulation to the EHD. It should be acknowledged that the synoptic circulation and contributing factors for this heat event may be unique for Typhoon Lekima and the SECC region. But TC induced subsidence warming and blocking of regular sea breeze might have occurred over other coastal regions too. Future studies examining other TC-heat events over other regions, such as Mexico and Central America, are strongly encouraged.

Climate models have projected increased intensity of TCs with global warming (Elsner et al., 2008; Knutson et al., 2016; Walsh et al., 2016). Accordingly, the severity of TC-related EHD might also increase and human society is likely to suffer more from more frequent severe TC-heat events in the future (Matthews

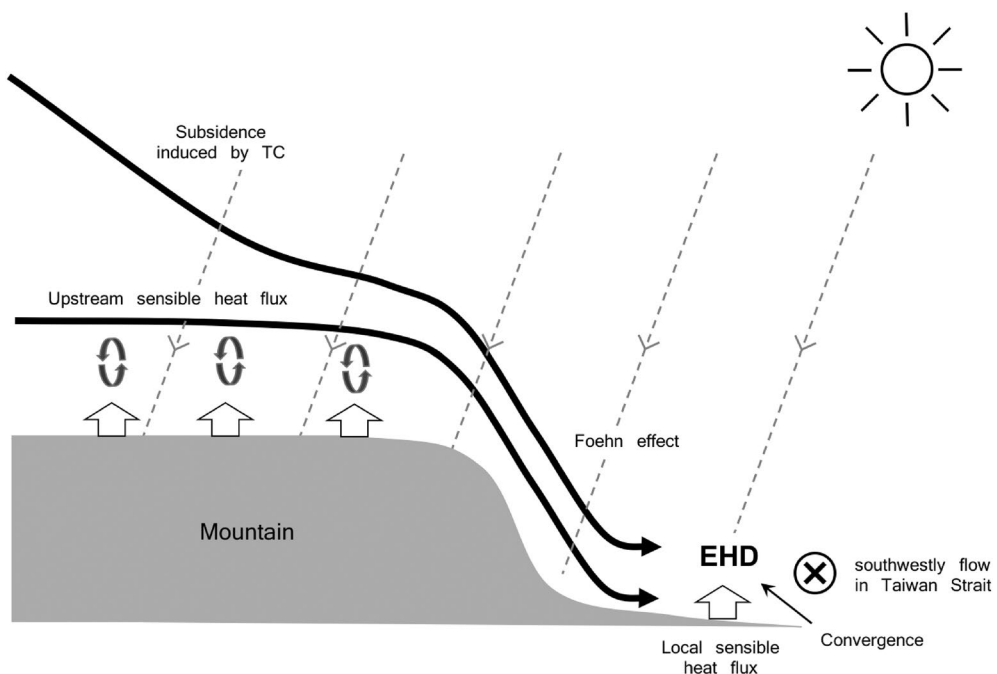


Figure 16. A schematic diagram summarizes TC-heat event formation mechanisms in the present study.

et al., 2019). The heat index (HI), a product of temperature and humidity, was an exposure metric in environmental health research and a more direct measure of heat effect on human health and comfort (Anderson et al., 2013; Matthews, 2018). A diagnosis and mechanism analysis of HI for TC-heat events would better describe potential risks as discussed in Matthews et al. (2019). An investigation of HI associated with Typhoon Lekima will be a focus in the future. In addition, the impact of urbanization and urban heat island effect, which could potentially enhance the strength of EHD (Luo & Lau, 2017; Zhou et al., 2019), also needs to be considered in future studies.

Acknowledgments

The authors gratefully acknowledge all the data centers for providing public access to the data products used in this study. The tropical cyclone best track data from Shanghai Typhoon Institute, China Meteorological Administration is acquired from http://tcdatalyphoon.org.cn/zjlsjj_zlhq.html. Meteorological station observations are obtained from the China Meteorological Data Sharing Service System (<http://cdc.cma.gov.cn/home.do>). National Centers for Environmental Prediction Final operational global analysis (NCEP FNL) data is obtained from <https://rda.ucar.edu/datasets/ds083.3/>. The authors would like to thank Ming Luo of Sun Yat-sen University and Yuya Takane of the National Institute of Advanced Industrial Science and Technology in Japan for their help in 2-m temperature evaluation and heat budget analysis, respectively. The authors also thank Jonathon S. Wright, Ping Lu and Danyang Wang for their help in improving this manuscript. This work was supported by the National Natural Science Foundation of China (41975127).

Conflict of Interest

The authors declare no conflicts of interest relevant to this study.

Data Availability Statement

All the simulation data and scripts used in this study are available at <https://cloud.tsinghua.edu.cn/d/e0e25f63fcf14bea8aa4/>.

References

- Ahn, Y.-I., & Lee, D. K. (2002). Impact of bogus tropical cyclones on summertime circulation in regional climate simulation. *Journal of Geophysical Research*, 107(D16). <https://doi.org/10.1029/2001jd000416>
- Anderson, G. B., Bell, M. L., & Peng, R. D. (2013). Methods to calculate the heat index as an exposure metric in environmental health research. *Environmental Health Perspectives*, 121(10), 1111–1119. <https://doi.org/10.1289/ehp.1206273>
- Arakane, S., & Hsu, H.-H. (2020). A tropical cyclone removal technique based on potential vorticity inversion to better quantify tropical cyclone contribution to the background circulation. *Climate Dynamics*, 54(5–6), 3201–3226. <https://doi.org/10.1007/s00382-020-05165-x>
- Bieli, M., Pfahl, S., & Wernli, H. (2015). A Lagrangian investigation of hot and cold temperature extremes in Europe. *Quarterly Journal of the Royal Meteorological Society*, 141(686), 98–108. <https://doi.org/10.1002/qj.2339>
- Black, E., Blackburn, M., Harrison, G., Hoskins, B., & Methven, J. (2004). Factors contributing to the summer 2003 European heatwave. *Weather*, 59(8), 217–223. <https://doi.org/10.1256/wea.74.04>
- Cha, D.-H., & Wang, Y. (2013). A dynamical initialization scheme for real-time forecasts of tropical cyclones using the WRF model. *Monthly Weather Review*, 141(3), 964–986. <https://doi.org/10.1175/mwr-d-12-00077.1>
- Chen, R., & Lu, R. (2015). Comparisons of the circulation anomalies associated with extreme heat in different regions of Eastern China. *Journal of Climate*, 28(14), 5830–5844. <https://doi.org/10.1175/jcli-d-14-00818.1>

- Chen, R., Wen, Z., Lu, R., & Wang, C. (2019). Causes of the extreme hot midsummer in central and South China during 2017: Role of the western tropical pacific warming. *Advances in Atmospheric Sciences*, 36(5), 465–478. <https://doi.org/10.1007/s00376-018-8177-4>
- Chen, T.-C., Wang, S.-Y., Yen, M.-C., Clark, A. J., & Tsay, J.-D. (2010). Sudden surface warming-drying events caused by typhoon passages across Taiwan. *Journal of Applied Meteorology and Climatology*, 49(2), 234–252. <https://doi.org/10.1175/2009jamc2070.1>
- Chen, X., Zhong, Z., Jiang, J., & Sun, Y. (2019). The impact of tropical cyclone activities over the western North Pacific on the large-scale regional circulation: A numerical investigation. *Chinese Journal of Geophysics-Chinese Edition*, 62(2), 489–498. <https://doi.org/10.6038/cjg2019M0017>
- Deng, K., Yang, S., Gu, D., Lin, A., & Li, C. (2020). Record-breaking heat wave in southern China and delayed onset of South China Sea summer monsoon driven by the Pacific subtropical high. *Climate Dynamics*, 54, 3751–3764. <https://doi.org/10.1007/s00382-020-05203-8>
- Ding, T., Qian, W., & Yan, Z. (2010). Changes in hot days and heat waves in China during 1961–2007. *International Journal of Climatology*, 30(10), 1452–1462. <https://doi.org/10.1002/joc.1989>
- Dong, W., Lin, Y., Wright, J. S., Xie, Y., Xu, F., Yang, K., et al. (2018). Connections between a late summer snowstorm over the Southwestern Tibetan Plateau and a Concurrent Indian Monsoon low-pressure system. *Journal of Geophysical Research - D: Atmospheres*, 123(24), 13676–13691. <https://doi.org/10.1029/2018jd029710>
- Elsner, J. B., Kossin, J. P., & Jagger, T. H. (2008). The increasing intensity of the strongest tropical cyclones. *Nature*, 455(7209), 92–95. <https://doi.org/10.1038/nature07234>
- Fischer, E. M. (2014). Autopsy of two mega-heatwaves. *Nature Geoscience*, 7(5), 332–333. <https://doi.org/10.1038/ngeo2148>
- Friedl, M. A., Sulla-Menashe, D., Tan, B., Schneider, A., Ramankutty, N., Sibley, A., & Huang, X. (2010). MODIS Collection 5 global land cover: Algorithm refinements and characterization of new datasets. *Remote Sensing of Environment*, 114(1), 168–182. <https://doi.org/10.1016/j.rse.2009.08.016>
- Gaffin, D. M. (2007). Foehn winds that produced large temperature differences near the southern Appalachian Mountains. *Weather and Forecasting*, 22(1), 145–159. <https://doi.org/10.1175/waf970.1>
- Hong, S.-Y., Noh, Y., & Dudhia, J. (2006). A new vertical diffusion package with an explicit treatment of entrainment processes. *Monthly Weather Review*, 134(9), 2318–2341. <https://doi.org/10.1175/mwr3199.1>
- Hsu, H.-H., Hung, C.-H., Lo, A.-K., Wu, C.-C., & Hung, C.-W. (2008). Influence of tropical cyclones on the estimation of climate variability in the tropical western North Pacific. *Journal of Climate*, 21(12), 2960–2975. <https://doi.org/10.1175/2007jcli1847.1>
- Huang, Z., Xiong, Y., & Lin, L. (2005). Analysis of synoptic characteristic and element related to Torrid weather of 37°C or more in Guangzhou. *Meteorological Monthly*, 31(7), 24–27.
- Iacono, M. J., Delamere, J. S., Mlawer, E. J., Shephard, M. W., Clough, S. A., & Collins, W. D. (2008). Radiative forcing by long-lived greenhouse gases: Calculations with the AER radiative transfer models. *Journal of Geophysical Research*, 113(D13). <https://doi.org/10.1029/2008jd009944>
- Ji, Z., Lin, G., Li, X., & Xiong, Y. (2005). High Temperature anomalies in Guangdong in summer 2003 and its climatic background. *Journal of Tropical Meteorology*, 21(2), 207–216.
- Knutson, T. R., McBride, J. L., Chan, J., Emanuel, K., Holland, G., Landsea, C., et al. (2016). Tropical cyclones and climate change. *Nature Geoscience*, 3(3), 157–163.
- Lam, H., Kok, M. H., & Shum, K. K. Y. (2012). Benefits from typhoons - The Hong Kong perspective. *Weather*, 67(1), 16–21. <https://doi.org/10.1002/wea.836>
- Li, Y., Lin, Y., & Wang, Y. (2019). A numerical study on the formation and maintenance of a long-lived rainband in Typhoon Longwang (2005). *Journal of Geophysical Research - D: Atmospheres*, 124(19), 10401–10426. <https://doi.org/10.1029/2019jd030600>
- Lin, N. (2019). Tropical cyclones and heatwaves. *Nature Climate Change*, 9(8), 579–580. <https://doi.org/10.1038/s41558-019-0537-2>
- Lin, N., & Emanuel, K. (2016). Grey swan tropical cyclones. *Nature Climate Change*, 6(1), 106–111. <https://doi.org/10.1038/nclimate2777>
- Luo, M., & Lau, N.-C. (2017). Heat waves in Southern China: Synoptic behavior, long-term change, and urbanization effects. *Journal of Climate*, 30, 703–720. <https://doi.org/10.1175/JCLI-D-16-0269.1>
- Matthews, T. (2018). Humid heat and climate change. *Progress in Physical Geography: Earth and Environment*, 42, 391–405. <https://doi.org/10.1177/030913318776490>
- Matthews, T., Wilby, R. L., & Murphy, C. (2019). An emerging tropical cyclone-deadly heat compound hazard. *Nature Climate Change*, 9(8), 602–606. <https://doi.org/10.1038/s41558-019-0525-6>
- Meehl, G. A., & Tebaldi, C. (2004). More intense, more frequent, and longer lasting heat waves in the 21st century. *Science*, 305(5686), 994–997. <https://doi.org/10.1126/science.1098704>
- Miralles, D. G., Teuling, A. J., van Heerwaarden, C. C., & Vilà-Guerau de Arellano, J. (2014). Mega-heatwave temperatures due to combined soil desiccation and atmospheric heat accumulation. *Nature Geoscience*, 7(5), 345–349. <https://doi.org/10.1038/ngeo2141>
- Mora, C., Dousset, B., Caldwell, I. R., Powell, F. E., Geronimo, R. C., Bielecki, C. R., et al. (2017). Global risk of deadly heat. *Nature Climate Change*, 7(7), 501–4. <https://doi.org/10.1038/nclimate3322>
- Parker, T. J., Berry, G. J., & Reeder, M. J. (2013). The influence of tropical cyclones on heat waves in Southeastern Australia. *Geophysical Research Letters*, 40, 6264–6270. <https://doi.org/10.1029/2013GL058257>
- Peduzzi, P., Chatenoux, B., Dao, H., De Boni, A., Herold, C., Kossin, J., et al. (2012). Global trends in tropical cyclone risk. *Nature Climate Change*, 2(4), 289–294. <https://doi.org/10.1038/nclimate1410>
- Perkins, S. E. (2015). A review on the scientific understanding of heatwaves-Their measurement, driving mechanisms, and changes at the global scale. *Atmospheric Research*, 164–165, 242–267. <https://doi.org/10.1016/j.atmosres.2015.05.014>
- Pfahl, S., & Wernli, H. (2012). Quantifying the relevance of atmospheric blocking for co-located temperature extremes in the Northern Hemisphere on (sub-)daily time scales. *Geophysical Research Letters*, 39. <https://doi.org/10.1029/2012gl052261>
- Shan, L. U., & Meng, Y. E. (2006). The research on relationship between outer circulation of tropical cyclones and high temperature weather in Guangzhou. *Journal of Tropical Meteorology*, 22(5), 461–465.
- Sheridan, P., Smith, S., Brown, A., & Vosper, S. (2010). A simple height-based correction for temperature downscaling in complex terrain. *Meteorological Applications*, 17(3), 329–339. <https://doi.org/10.1002/met.177>
- Sherwood, S. C., & Huber, M. (2010). An adaptability limit to climate change due to heat stress. *Proceedings of the National Academy of Sciences*, 107(21), 9552–9555. <https://doi.org/10.1073/pnas.091352107>
- Shibata, Y., Kawamura, R., & Hatushika, H. (2010). Role of large-scale circulation in Triggering Foehns in the Hokuriku District of Japan during Midsummer. *Journal of the Meteorological Society of Japan. Ser. II*, 88(3), 313–324. <https://doi.org/10.2151/jmsj.2010-304>
- Skamarock, W. C., Klemp, J. B., Dudhia, J., Gill, D. O., Barker, D. M., Duda, M. G., et al. (2008). *A Description of the Advanced research WRF version 3*. <https://doi.org/10.5065/D68S4MVH>

- Sprenger, M., & Wernli, H. (2015). The LAGRANTO Lagrangian analysis tool - Version 2.0. *Geoscientific Model Development*, 8(8), 2569–2586. <https://doi.org/10.5194/gmd-8-2569-2015>
- Takane, Y., & Kusaka, H. (2011). Formation mechanisms of the extreme high surface air temperature of 40.9°C observed in the Tokyo Metropolitan Area: Considerations of dynamic Foehn and Foehnlike Wind. *Journal of Applied Meteorology and Climatology*, 50(9), 1827–1841. <https://doi.org/10.1175/jamc-d-10-05032.1>
- Takane, Y., Kusaka, H., & Kondo, H. (2015). Investigation of a recent extreme high-temperature event in the Tokyo metropolitan area using numerical simulations: The potential role of a 'hybrid' foehn wind. *Quarterly Journal of the Royal Meteorological Society*, 141(690), 1857–1869. <https://doi.org/10.1002/qj.2490>
- Thompson, G., Field, P. R., Rasmussen, R. M., & Hall, W. D. (2008). Explicit forecasts of winter precipitation using an improved bulk microphysics scheme. Part II: Implementation of a New Snow Parameterization. *Monthly Weather Review*, 136(12), 5095–5115. <https://doi.org/10.1175/2008mwr2387.1>
- Walsh, K. J. E., McBride, J. L., Klotzbach, P. J., Balachandran, S., Camargo, S. J., Holland, G., et al. (2016). Tropical cyclones and climate change. *Wiley Interdisciplinary Reviews: Climate Change*, 7(1), 65–89. <https://doi.org/10.1002/wcc.371>
- Wang, L., & Li, D. (2019). Modulation of the urban boundary-layer heat budget by a heatwave. *Quarterly Journal of the Royal Meteorological Society*, 145(722), 1814–1831. <https://doi.org/10.1002/qj.3526>
- Wang, W., Zhou, W., Li, X., Wang, X., & Wang, D. (2016). Synoptic-scale characteristics and atmospheric controls of summer heat waves in China. *Climate Dynamics*, 46(9–10), 2923–2941. <https://doi.org/10.1007/s00382-015-2741-8>
- Wernli, H., & Davies, H. C. (1997). A Lagrangian-based analysis of extratropical cyclones. I: The method and some applications. *Quarterly Journal of the Royal Meteorological Society*, 123(538), 467–489. <https://doi.org/10.1256/smsqj.53810>
- Xu, K.-M., & Randall, D. A. (1996). A semimipirical cloudiness parameterization for use in climate models. *Journal of the Atmospheric Sciences*, 53(21), 3084–3102. [https://doi.org/10.1175/1520-0469\(1996\)053<3084:ascpfu>2.0.co;2](https://doi.org/10.1175/1520-0469(1996)053<3084:ascpfu>2.0.co;2)
- Yan, Z., Xingyu, Z., Yi, L., Yanping, Z., & Shan, G. (2001). Cause of high-temperature weather in summer in Fujian Province. *Meteorological Monthly*, 09, 26–30.
- Ying, M., Zhang, W., Yu, H., Lu, X., Feng, J., Fan, Y., et al. (2014). An overview of the China meteorological administration tropical cyclone database. *Journal of Atmospheric and Oceanic Technology*, 31(2), 287–301. <https://doi.org/10.1175/jtech-d-12-00119.1>
- Zhang, L., Shen, S., & Sun, X. (2010). Quantitative estimation of high temperature under the influence of outer circulation of tropical cyclones in Shenzhen. *Meteorological Monthly*, 36(4), 37–42.
- Zhang, Z., Wang, Y., Zhang, W., & Xu, J. (2019). Coastal ocean response and its feedback to Typhoon Hato (2017) over the South China Sea: A numerical study. *Journal of Geophysical Research - D: Atmospheres*, 124(24), 13731–13749. <https://doi.org/10.1029/2019jd031377>
- Zhong, Z., Chen, X., Yang, X.-Q., Ha, Y., & Sun, Y. (2019). The relationship of frequent tropical cyclone activities over the western North Pacific and hot summer days in central-eastern China. *Theoretical and Applied Climatology*, 138, 1395–1404. <https://doi.org/10.1007/s00704-019-02908-7>
- Zhou, C., Wang, K., Qi, D., & Tan, J. (2019). Attribution of a Record-Breaking Heatwave Event in Summer 2017 over the Yangtze River Delta. *Bulletin of the American Meteorological Society*, 100(1), S97–S103. <https://doi.org/10.1175/bams-d-18-0134.1>
- Zscheischler, J., Martius, O., Westra, S., Bevacqua, E., Raymond, C., Horton, R. M., et al. (2020). A typology of compound weather and climate events. *Nature Reviews Earth & Environment*, 1(7), 333–347. <https://doi.org/10.1038/s43017-020-0060-z>
- Zscheischler, J., Westra, S., van den Hurk, B. J. J. M., Seneviratne, S. I., Ward, P. J., Pitman, A., et al. (2018). Future climate risk from compound events. *Nature Climate Change*, 8(6), 469–477. <https://doi.org/10.1038/s41558-018-0156-3>